HAL
archives-ouvertes.fr

Definition of a 4D Continuous Polar Transformation for the Tracking and the Analysis of LV Motion

Jérôme Declerck, Jacques Feldmar, Nicholas Ayache

▶ **To cite this version:**

Jérôme Declerck, Jacques Feldmar, Nicholas Ayache. Definition of a 4D Continuous Polar Transformation for the Tracking and the Analysis of LV Motion. RR-3039, INRIA. 1996. <inria-00073654>

HAL Id: inria-00073654
https://hal.inria.fr/inria-00073654

Submitted on 24 May 2006

HAL is a multi-disciplinary open access archive for the deposit and dissemination of scientific research documents, whether they are published or not. The documents may come from teaching and research institutions in France or abroad, or from public or private research centers.

L'archive ouverte pluridisciplinaire **HAL**, est destinée au dépôt et à la diffusion de documents scientifiques de niveau recherche, publiés ou non, émanant des établissements d'enseignement et de recherche français ou étrangers, des laboratoires publics ou privés.

INSTITUT NATIONAL DE RECHERCHE EN INFORMATIQUE ET EN AUTOMATIQUE

Definition of a 4D continuous polar transformation for the tracking and the analysis of LV motion

Jérôme Declerck, Jacques Feldmar, Nicholas Ayache

N° 3039

Novembre 1996

THÈME 3

ISSN 0249-6399

INRIA
SOPHIA ANTIPOLIS

Definition of a 4D continuous polar transformation for the tracking and the analysis of LV motion

Jérôme Declerck[*] , Jacques Feldmar, Nicholas Ayache

Thème 3 — Interaction homme-machine,
images, données, connaissances
Projet Epidaure[**]

Rapport de recherche n ° 3039 — Novembre 1996 — 34 pages

Abstract:

Cardiologists assume that analysis of the motion of the heart (especially the left ventricle) can give precise information about the health of the myocardium.

A 4D polar transformation is defined to describe the left ventricle (LV) motion and a method is presented to estimate it from sequences of 3D images. The transformation is defined in 3D-planispheric coordinates by a small number of parameters involved in a set of simple linear equations. It is continuous and regular in time and space, periodicity in time can be imposed. The local motion can be easily decomposed into a few canonical motions (centripetal contraction, rotation around the long-axis, elevation). To recover the motion from original data, the 4D polar transformation is calculated using an adaptation of the Iterative Closest Point algorithm.

We present the mathematical framework and a demonstration of its feasability on a set of synthetic but realistic datapoints, simulating the motion of the LV and on a gated SPECT sequence.

Key-words: non-rigid matching, 4D, medical image, cardiology.

(Résumé : tsvp)

[*] E-mail: Jerome.Declerck@sophia.inria.fr
[**] http://www.inria.fr/Equipes/EPIDAURE-eng.html

Unité de recherche INRIA Sophia-Antipolis
2004 route des Lucioles, BP 93, 06902 SOPHIA-ANTIPOLIS Cedex (France)
Téléphone : 04 93 65 77 77 – Télécopie : 04 93 65 77 65

Définition d'une fonction polaire continue 4D pour le suivi et l'analyse du mouvement du ventricule gauche

Résumé : Les cardiologues supposent que l'analyse du mouvement du muscle cardiaque (plus précisément, du ventricule gauche) peut donner des informations locales sur la santé du myocarde.

Nous définissons une classe de transformations de l'espace et du temps (transformations polaires 4D) pour décrire le mouvement du ventricule gauche et nous présentons une méthode pour estimer une telle transformation à partir d'une séquence d'images tridimensionnelles. Cette transformation est définie en coordonnées planisphériques 3D par un nombre réduit de paramètres et par des relations linéaires simples. La transformation est continue et régulière dans l'espace et le temps, la périodicité temporelle peut être imposée implicitement. Le mouvement local d'un point du myocarde peut être facilement décomposé en mouvements élémentaires canoniques (contraction centripétale, rotation autour de l'axe long, élévation). Pour retrouver le mouvement à partir des images, la transformation polaire 4D est calculée grâce à une adaptation à notre problème 4D de l'algorithme du Point le Plus Proche Itératif.

Nous décrivons le contexte mathématique et une démonstration de sa faisabilité sur un exemple synthétique (mais réaliste) simulant le mouvement du ventricule gauche et sur une séquence SPECT synchronisée à l'ECG.

Mots-clé : mise en correspondance non-rigide, 4D, image médicale, cardiologie.

Introduction

Cardiologists assume that the analysis of the motion of the heart (especially the left ventricle) can give precise information about the health of the myocardium. A huge effort has been made in medical image processing to track and analyse the motion of the LV, but due to the complexity of the modeling, this topic remains an open research problem.

Modern techniques provide 3D images which describe either the anatomy of the heart (MRI, for instance) or its functionality (Nuclear Medicine SPECT imaging, for instance). It is possible to get sequences of such images over the whole cardiac cycle; such sequences are real 3D movies of the motion of the heart. The cardiac motion, like the motion of any real object must be therefore described as a 4D continuous and regular transformation of time and space.

Many techniques have been proposed to track the LV motion. All of them attempt to find the correspondence between pairs of successive images. Most of the proposed methods in 3D define a model of the shape of LV surfaces (endocardium and/or epicardium), using classical snake-like models [1, 23], spring-mass meshes [17] or more constrained generic surfaces such as free-deformed superquadrics [3, 4] or volumetric superquadrics [19, 18]. The tracking is processed using conservation constraints based on proximity constraints [3, 4], differential properties of the surface [1, 7, 11, 23] or is directly computed from displacement or velocity information obtained in some specific MR imaging techniques: tags [9, 13, 19, 21, 27] or phase contrast [15, 24]. In other work, no shape model is computed: the tracking is processed directly from the volumetric image using conservation of differential elements of isophotes [5] or using similarities of the intensity levels [25].

Unfortunately, because the correspondence is defined between two successive images, regularity and periodicity in time is not guaranteed. Only a few studies in 2D [26, 14] or in 3D [17, 25] perform a posteriori time filtering. Moreover, these methods ([19, 18] excepted) do not provide intuitive parameters describing characteristic motions without non-trivial computation [3, 4, 28]. The 4D polar transformation defined in this article aims to achieve four goals:

1. to define a class of transformation of **time** and **space** in which the **temporal continuity and periodicity** are included,

2. to define a class of **highly constrained** transformations in order to have a **relevant** description of the LV motion with a **minimal** number of parameters,

3. to be able to retrieve canonical motions with minimal computation, providing an easy-to-interpret **quantitative analysis** of the motion.

4. last, but not least, to be a transformation which combines the unknown parameters **in a linear way** to make their estimation easier and robust.

We shall see that all these points are achieved in the mathematical formulation that we propose below.

The paper is organised as follows: in section 1, we define the 4D polar transformation and the way to estimate it from a 4D (3D + time) data set. In section 2, a method is proposed to track in 4D the motion of the LV. Experiments have been conducted with a synthetic heart model and a gated SPECT sequence are presented in section 3. Section 4 draws conclusions concerning this work, its potential uses and future perspectives.

1 Definition of the 4D polar transformation

The idea of this study is to define a continuous and regular transformation of time and space. This transformation should also be adapted to describe with a minimum of parameters a complex motion such as the LV motion. This model of the deformation of the LV is a crude approximation compared to complex biomechanical models [12] or highly descriptive kinematic models [2].

Given a point M (x, y, z) in cartesian coordinates and a time value t, the transformation gives a point N (x', y', z') which is assumed to be the location of point M at time t. The cardiac motion is supposed to be regular in space and periodic in time. We therefore look for a **differentiable** function in spatial variables x, y and z and for a **differentiable** and **periodic** function in time variable t.

$$\begin{array}{rcl} f : \mathbb{R}^3 \times \mathbb{R} & \longrightarrow & \mathbb{R}^3 \\ (M, t) & \longmapsto & N = f(M, t) \end{array}$$

This definition of the 4D transformation yields the definition of 2 categories of functions which are easier to understand and which are intrinsically regular:

$$\begin{array}{rcll} Traj_M & = & f(M, \cdot) & \text{is the trajectory of } M \text{ over time,} \\ Deform_t & = & f(\cdot, t) & \text{is the transformation function of the object at time } t. \end{array}$$

In this paper, f is defined in order to describe locally some specific motions of points on the myocardium. We approximate the shape of the left ventricle as a stretched sphere in the long-axis direction. This is, of course, a very crude approximation as the shape of the heart is much more complex, however our goal is not a precise definition of the shape of the muscle, but a plausible discrimination of characteristic motions.

For that particular purpose, we separate the motion of a point of the heart into three canonical orthogonal motions (Fig. 1):

- motion 1: a **centripetal motion** which decribes the contraction or dilatation of the whole structure towards a "center",

- motion 2: a **apico-basal rotation** around the apico-basal axis which describes the twisting motion of the LV points,
- motion 3: a motion (tangential to the surface $r = C^t$) which describes the **elevation** of the LV points in the apico-basal direction (the shortening of apex-base distance during the systole).

We describe these motions in a "3D-planispheric" coordinates, which is a combination of spherical and cylindrical coordinates. Our tranformation function is thus defined as a composition of three functions:

$$f \quad = \quad P2C \circ F \circ C2P$$

The function $C2P$ switches from cartesian to 3D-planispheric coordinates, $P2C$ switches back from 3D-planispheric to cartesian coordinates (of course, $C2P = P2C^{-1}$). F is the function which is described with the three basic motions in 3D-planispheric coordinates. The next two paragraphs detail the definitions of these functions.

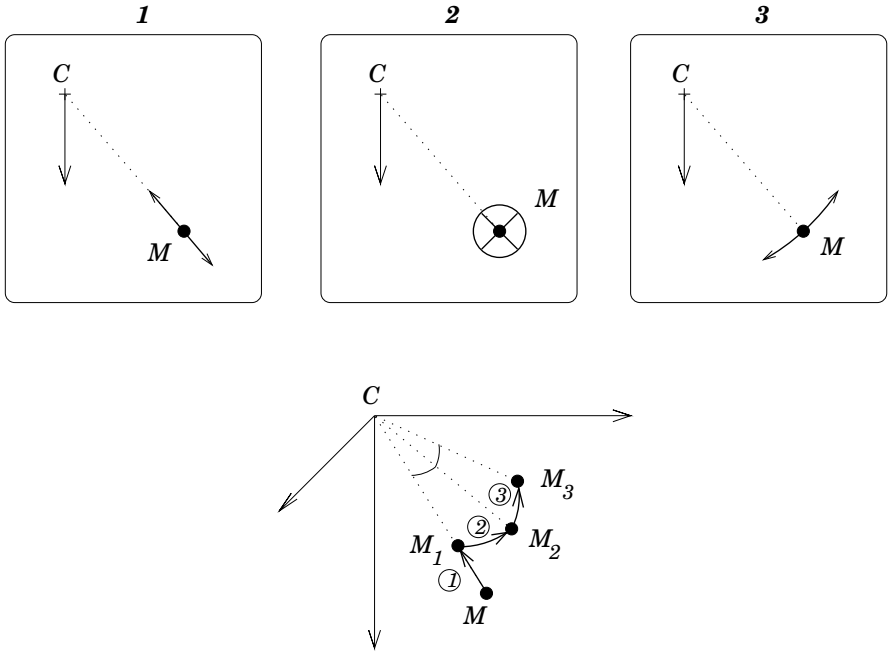

Figure 1: The top three frames illustrate the orthogonal motions described in the text. Bottom, point M is transformed in M_1 by the first motion (centripetal contraction), M_1 is transformed in M_2 by the second (apico-basal rotation) and M_2 is transformed in M_3 by the third one (elevation).

1.1 Cylindrical or planispheric coordinates ?

The approach is inspired from [18, 19]: in that study, the equations for the deformation of the superquadric model is expressed in cylindrical coordinates. In such coordinates, the decomposition of the local motion in our three canonical motions does not have the same relevance if the point where they are estimated belongs to a lateral wall (where the muscle is roughly cylindrical) or if the point is close to the apex (where the muscle is roughly spherical). For instance, a point belonging to a lateral wall and animated by an axial contraction does effectively contract towards the cylindrical axis (motion 1), but a point close to the apex animated with a similar motion does not contract, but undergoes a shift tangential to the wall. Thus, this motion is a twist (motion 2) or an elevation (motion 3) rather than a contraction (motion 1) (Fig. 2).

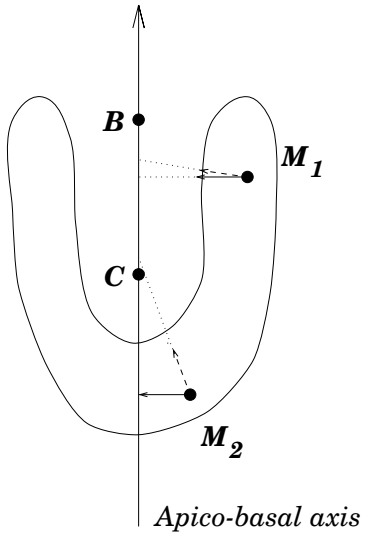

Figure 2: M_1 belongs to a lateral wall, M_2 is close to the apex, both points are animated with motion 1. Solid arrows describe the motion in cylindrical coordinates (contraction towards the apico-basal axis) and dotted arrows describe the motion in spherical coordinates (contraction towards the center C). Motion 1 effectively describes a contraction for M_1, but not for M_2.

We find it easier to use 3D-planispheric coordinates rather than cylindrical ones to decompose the local motion of points of the myocardium.

1.2 3D-Planispheric coordinates

C2P : in 3D cartesian space, we define a 3D-planispheric reference system given a center C, a base B and a set of two orthogonal vectors $\boldsymbol{u}$ and $\boldsymbol{v}$ (Fig. 3). In order to fit with our

description of the heart, we choose $\boldsymbol{u}$ as a vector parallel to the apico-basal direction, and $\boldsymbol{v}$ parallel to the septo-lateral direction. C is chosen in the center of the cavity, and B in the center of the base.

For each point M (x, y, z), a center point H_M is defined on line (CB). From this center point, a distance and two angles (latitude θ and longitude ϕ) are calculated just as in the classical spherical coordinate system. In the spherical system, H_M is the center C. In the cylindrical system, H_M is the orthogonal projection of M on the line CB. Our purpose here is to define a **combination of both spherical and cylindrical** coordinate systems, in order to describe the position of M in "roughly" spherical coordinates around the apex (where the shape of the LV is roughly spherical) and in "roughly" cylindrical coordinates around the base (where the shape of the LV is roughly cylindrical). In our system, the position of H_M on the line CB is given by the simple formula:

$$\boldsymbol{CH_M} = (1 - cos\theta)\,\boldsymbol{CB} \tag{1}$$

- For low values of θ (M around the apex), H_M is close to C and shifts away from C with a distance increasing with $\frac{\theta^2}{2}$: around the apex, the 3D-planispheric coordinate system is thus close to the spherical one.
- For θ around $\frac{\pi}{2}$ (M around the apex), H_M is close to B, the distance BH_M varies linearly with $\theta - \frac{\pi}{2}$, and $\boldsymbol{MH_M}$ is nearly orthogonal to $\boldsymbol{CB}$: around the base, the 3D-planispheric system is close to the cylindrical one (Fig. 3).

Of course, (1) is an implicit formula: H_M gives the angle θ, but we need θ to locate H_M. Appendix A details the method we have developed to compute the location of H_M given a point M in space.

In our 3D-planispheric system, a surface ($r =$ Constant) is represented as a disk in a plane, like in a classical map projection in topography (this is why we use the word "planispheric"). The coordinates X, Y and R in this system are defined as follows:

$$\begin{aligned} X &= \frac{\theta}{\pi}\, cos(\phi) \\ Y &= \frac{\theta}{\pi}\, sin(\phi) \\ R &= \frac{r}{\sigma_r} \end{aligned} \tag{2}$$

where σ_r is a normalization coefficient so that X, Y and R are dimensionless and vary within a similar range of values.

Fig. 4 illustrates the correspondence between the (x, y, z) cartesian coordinates and the (X, Y, R) coordinates in the planispheric system. In this system, point ($X = 0$, $Y = 0$) is

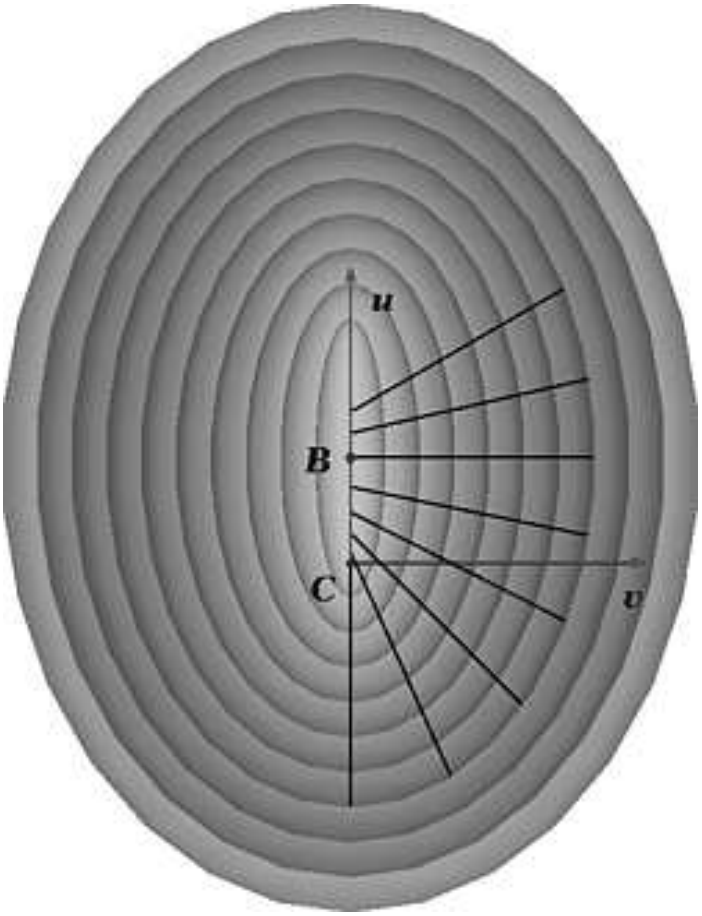

Figure 3: A representation of ten surfaces ($r = C^t$). The black lines show different points M and their associated center H_M.

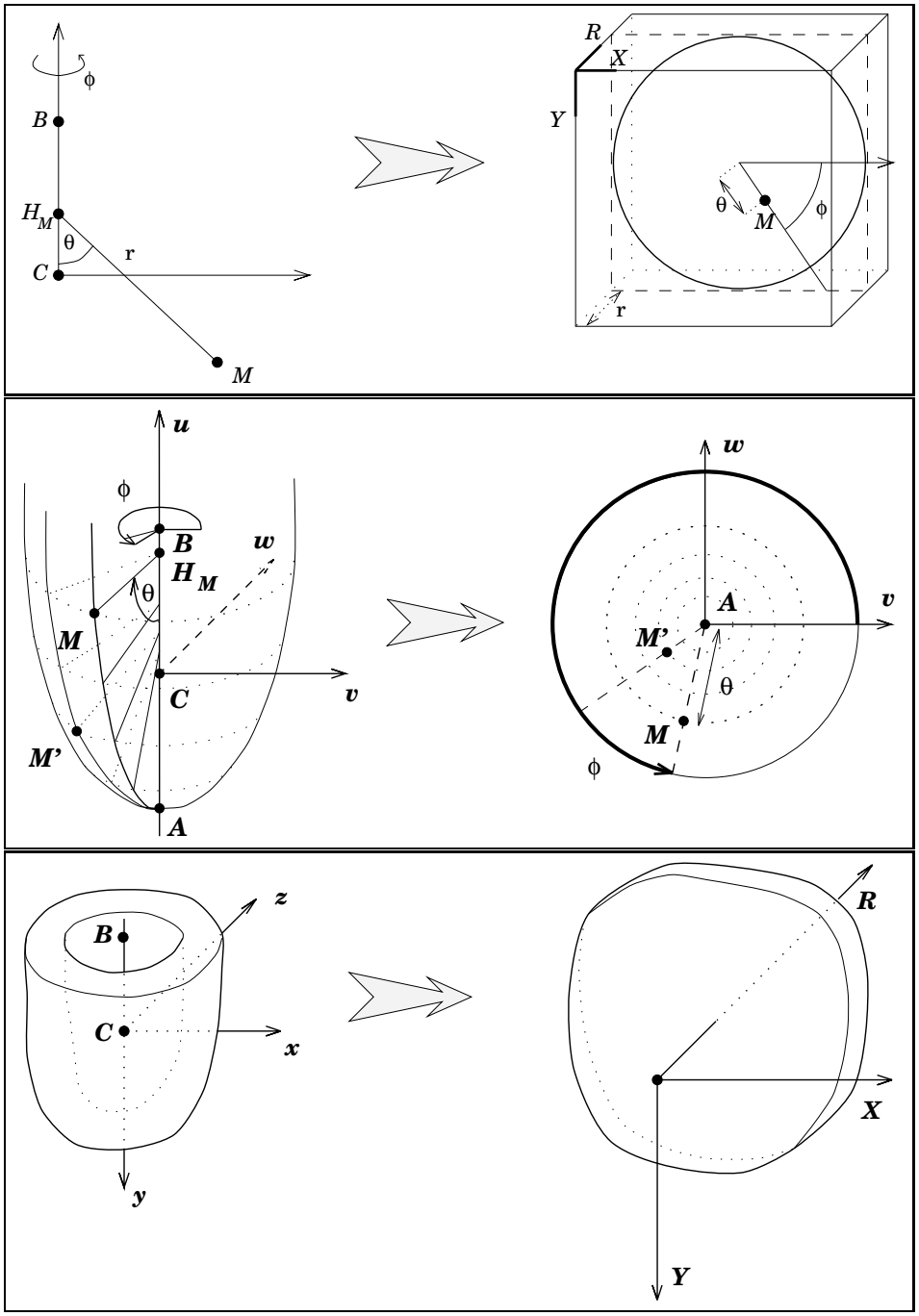

Figure 4: **Top**, the (x,y,z) cartesian location of the point M is converted into polar coordinates in the 3D-planispheric image, the depth R is the distance from the point H_M in the cartesian image, the position (X,Y) in the plane is defined with the two angles θ and ϕ, like in the 2D-planispheric mapping. **Middle**, for a constant value of r, like in planispheric projection, parallels (θ constant) become concentric circles and meridians (ϕ constant) become segments starting from the center of the disc. **Bottom**, the shape of the heart is roughly a plate in the 3D-planispheric coordinate system.

the "south pole" of the projection[1], the points on the circle $X^2 + Y^2 = 1$ ($\theta = \pi$) are the same cartesian point, the "north pole" of the projection. Around this point, the distorsion between the cartesian and our planispheric representation is maximum, but there should not be any cardiac points in this area (Fig. 5).

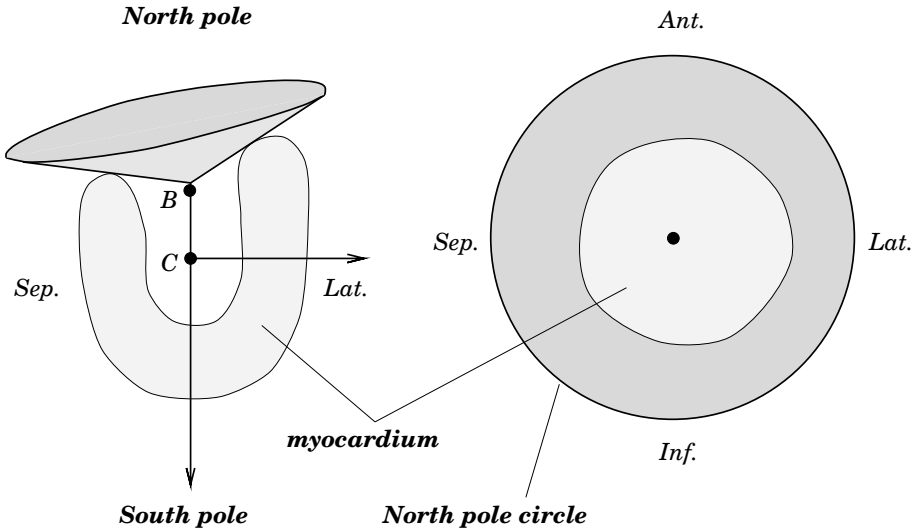

Figure 5: Left, the myocardium. From the center C, the limit of the basis draws a cone (dark gray) around the north pole. Right, in the 3D planispheric map, the left ventricle (light gray) appears like a plate, the cone is a circular stripe around the heart.

P2C : conversely, given a point (X, Y, R) in the planispheric system so that $X^2+Y^2 \leq 1$, we can compute its cartesian coordinates (x, y, z) by calculating $\theta = \pi\sqrt{X^2+Y^2}$ and ϕ without ambiguity with the expressions of $cos(\phi)$ and $sin(\phi)$. The center H_M is calculated with (1).

1.3 The function in 3D-planispheric coordinates

In the planispheric system, given a point M (X, Y, R), the transformed point N (X', Y', R') through F is expressed as follows:

$$\begin{aligned} X' &= a_0X - a_1Y + a_2 \\ Y' &= a_1X + a_0Y + a_3 \\ R' &= a_4R + a_5 \end{aligned} \tag{3}$$

[1]this south pole should be the apex

X' and Y' are defined by a similitude function[2] applied to X and Y. R' is defined as an affine function of R. The similitude and the affine parameters are continuous and differentiable functions of r, θ, ϕ and t.

Defining the transformation in the 3D-planispheric coordinate system yields: a) linear expressions in the parameters a_p, b) a simple computation of the canonical motion decomposition (centripetal contraction, rotation, elevation) from the a_p parameters and, c) a very compact description of the deformation.

1.3.1 Analysis of the motion in the canonical decomposition

Our canonical motions are retrieved with the following formulae:

1. the **centripetal contraction** ratio (motion 1) is given by:

$$\frac{R'}{R} = a_4 + \frac{a_5}{R} \tag{4}$$

2. the linear relationships between X', Y' and X, Y define a 2D similitude such that

$$k = \sqrt{a_0^2 + a_1^2} \tag{5}$$

$$\alpha = atan2(\frac{a_1}{k}, \frac{a_0}{k}) \tag{6}$$

   α is the **rotation** around the apico-basal axis (motion 2).

3. k is the scale factor corresponding to an elevation magnification in latitude, which is our motion 3. In our display, we compute $\frac{\theta' - \theta}{\theta}$.

The 4D polar transformation is defined once the parameters a_i are determined. Because of the simplicity of (5) and (6), it is possible to easily analyse the motion using the parameters a_i. Because the variation of the parameters a_i is smooth and regular with variables r, θ, ϕ and t, the parameters which describe our canonical motions are also smooth and regular in time and space.

1.3.2 Degrees of freedom of the parameters, time dependency as a hard constraint

In order to define a smooth and continuous 4D transformation, the parameters depend on the location of the point and the instant at which the transformation is calculated. In our

[2] a combinate of a 2D rotation by angle α, a uniform scaling of ratio k and a translation

formulation, we choose the parameters as polynomial functions in r and θ and quadratic periodic B-splines in ϕ and t:

$$a_p(r,\theta,\phi,t) = \sum_{i=0}^{n_r-1} \sum_{\substack{j=0 \\ j\neq 1}}^{n_\theta} \sum_{k=0}^{n_\phi-1} \sum_{n=0}^{n_t-1} A^p_{i,j,k,n} \left(\frac{r}{\sigma_r}\right)^i \left(\frac{\theta}{\pi}\right)^j B^\Phi_k(\phi)\, B^T_n(t) \tag{7}$$

for $p = 0 \ldots 4$. If we keep for a_5 an expression like (7), a_4 and a_5 are correlated because $R = \frac{r}{\sigma_r}$. We therefore simplify a_5 as follows:

$$a_5(r,\theta,\phi,t) = \sum_{\substack{j=0 \\ j\neq 1}}^{n_\theta} \sum_{k=0}^{n_\phi-1} \sum_{n=0}^{n_t-1} A^5_{j,k,n} \left(\frac{\theta}{\pi}\right)^j B^\Phi_k(\phi)\, B^T_n(t) \tag{8}$$

with the following notation:

- n_r is the number of parameters which define the polynomial function of variable r: the degree of this polynomial is $n_r - 1$.
- n_θ is the number of parameters which define the polynomial function of variable θ: to be differentiable in points for which $(\theta = 0)$, the polynomial must have no term in θ $(a_p(\theta) = a^0_p + a^2_p\theta^2 + a^3_p\theta^3 \ldots)$. a_p is therefore a polynomial of θ of degree n_θ.
- n_ϕ is the number of control points of the B-spline periodic curve of variable ϕ. B^Φ are the B-spline basis functions associated to a classical regularly distributed 2π-periodic set of knots [22].
- n_t is the number of control points of the B-spline curve of variable t. B^T are the B-spline basis functions associated to a classical regularly distributed set of knots, this basis can be periodic or not.

The originality of the transformation is in the fact that the continuity and potentially the periodicity in time is a "hard" constraint. We can **implicitly look for time-periodic transformations**.

Using quadratic B-splines (with a set of regularly distributed knots in our current implementation) ensures $\mathcal{C}^1$ continuity in ϕ and t; the function $a_p(r,\theta,\phi,\cdot)$ is a (potentially periodic) piecewise polynomial. Due to the definition of B-splines, the influence of possible outliers remain local [22].

To ensure the continuity for $\theta = 0$, we must impose the constraint $A^p_{i,0,k,n} = A^p_{i,0,0,n}$ for each k. There are thus $n_\phi - 1$ equations for each i and n. Finally, we get a number of control points equal to $(5.n_r + 1).(n_\phi.(n_\theta - 1) + 1).n_t$.

The transformation is completely defined given a center C and two orthogonal vectors (they define the 3D-planispheric system) and a set of control points (real numbers) $A^p_{i,j,k,n}$.

1.4 Estimation of a 4D planispheric transformation

1.4.1 The least squares criterion

Having a set of matches (M_l, $N_{n,l}$) for different times t_n ($n = 0 \dots T-1$), we define a least squares criterion to estimate the 4D planispheric transform which could "best" fit the list of matches:

$$\forall n \in 0 \dots T-1, \forall l \in 0 \dots N-1,$$

$$f(M_l, t_n) \simeq N_{n,l} \tag{9}$$

The least squares criterion is therefore written:

$$J(f) = \sum_{n=0}^{T-1} \sum_{l=0}^{N-1} \alpha_{n,l} \, . \, d(\, f(M_l, t_n) \, ; \, N_{n,l} \,)^2 \tag{10}$$

where $d(\cdot;\cdot)$ is the distance and $\alpha_{n,l}$ is the weight related to the reliability of the match (M_l, $N_{n,l}$).

If we choose the euclidean distance for d in cartesian coordinates, the criterion is not quadratic in the $A^p_{i,j,k,n}$, and its derivatives with respect to the $A^p_{i,j,k,n}$ are very difficult to linearize. We prefer to choose for d the euclidean distance expressed in planispheric coordinates ($X^2 + Y^2 + R^2$). The criterion is then quadratic in the $A^p_{i,j,k,n}$. d is a distance if and only if $X^2 + Y^2 < 1$ (i.e. iff (X,Y) does not belong to the circle of the "north pole" of the planispheric map). As soon as the center C is well inside the cavity and the base point B is in the center of the base circle, we are sure that all data points remain in a "security" cylinder in the 3D-planispheric system (maximum expected value for θ is around $\pi/2$). See fig. 5).

1.4.2 Minimization of the criterion

The criterion expressed with d as the euclidean distance in planispheric coordinates is quadratic in the control points $A^p_{i,j,k,n}$. Differentiating it with respect to $A^p_{i,j,k,n}$ gives a linear system which is solved with a classical conjugate gradient method. The size of the matrix is $(5.n_r + 1).(n_\phi.(n_\theta - 1) + 1).n_t$. In fact, the linear system can be split in two independent subsystems, one for a_0, a_1, a_2, a_3 and the other for a_4 and a_5.

2 Tracking the 4D motion of the LV

We define in this section an adaptation of the Iterative Closest Point algorithm [6, 29] which gives an estimation of those matches for the least squares minimization: it is possible this way to calculate the "best" function with respect to a distance criterion.

The motion is tracked in a heart image sequence (in our experiments, gated SPECT). Points featuring the edges of the heart are extracted and matched. The result of the matches between pairs of points in the images of the sequence is used to estimate a 4D polar transformation.

2.1 Matching the feature points

The matching method is an enhancement of the iterative closest point [6, 29, 10], adapted to our problem. Given a point M (x, y, z) in cartesian coordinates and a time value t, the transformation gives a point N (x', y', z') which is assumed to be the location of point M at time t. To estimate a 4D planispheric transformation f, we therefore need to know the matches between points M_l of the first image ($t = 0$) and points $N_{n,l}$ of the image at time n ($t = t_n$). Thus, we look for f so that

$$f(M_l, t_n) \simeq N_{n,l}$$

We define a criterion:

$$C(f) = \sum_{n=0}^{T-1} \sum_{l=0}^{N-1} \alpha_{n,l} \, . \, d[\, f(M_l, t_n) \, ; \, \mathrm{CP}_n(f(M_l, t_n)) \,]^2. \tag{11}$$

CP_n calculates the closest point to a 3D point among the feature points FP_n extracted in image n. The criterion is the sum of the residual distances between the estimated location of the points M_l at time t_n and the feature points extracted in Image n. $\alpha_{n,l}$ is a weighting coefficient which depends only on (M_l, t_n) (Fig. 6).

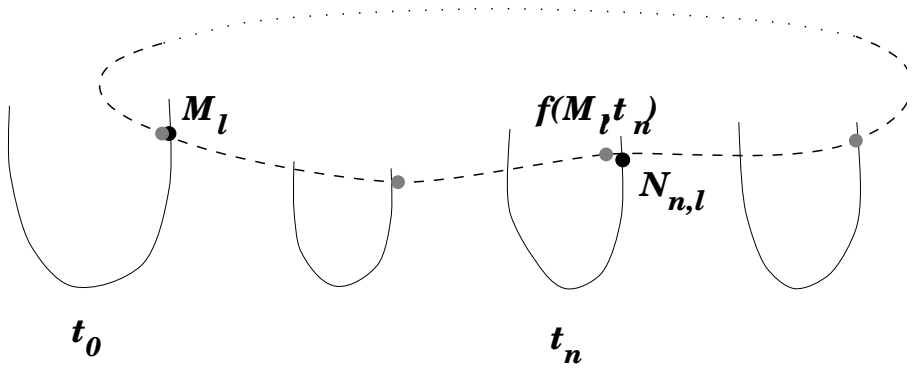

Figure 6: The matching criterion measures the sum of distances between $f(M_l, t_n)$, the estimated point M_l at time t_n and $N_{n,l}$, the closest feature point of Image n, for all existing M_l and t_n.

2.2 Minimizing the criterion

The minimization process is iterative, given an initial transformation f_0. This initial transformation is chosen in our experiments to be the identity (nothing moves anywhere !). Each iteration k splits into three steps:

1. For each 4D point (M_l, t_n), we calculate $f_{k-1}(M_l, t_n)$ (which should be the location of point M_l at time t_n) and we identify its closest feature point $CP_{n,l}$ in Image n. We therefore end up with a list of possible matched pairs of points.

2. For each time t_n and for each type of boundary (endocardium, epicardium), we calculate the residual distance $\|f_{k-1}(M_l, t_n) - CP_{n,l}\|$ for each pair, and we decide whether a pair is reliable or not: we first eliminate pairs for which the residual distance exceeds a fixed threshold. Second, we compute the mean μ and the standard deviation σ attached to the remaining pairs. We then eliminate the points for which the distance is greater than another threshold depending on the distance distribution ($\mu + c.\sigma$, where c can be easily set using a χ^2 table [10]).

   We get for this iteration a list S_k of reliable pairs of matched points. Notice that if a point is not matched in this iteration, it may be matched in one that follows.

3. With the filtered list S_k of pairs of points, we calculate f_k which is the best least squares fit for the pairs of points.

The iterative process stops when a maximum number of iterations is reached, or when $S_k = S_{k-1}$. [10] gives further details about this adaptation of the iterative closest point algorithm, for instance about the convergence properties.

2.3 Definition of the closest point

The matching function $ClosestPointOnFP_n$ takes into account for each point its geometric position and the local direction of the intensity gradient calculated while extracting the edges. Considering 2 points M and N and their intensity gradient vectors $\boldsymbol{n}_M$ and $\boldsymbol{n}_N$ respectively, the distance between them is calculated as follows:

$$d(M,N)^2 = \alpha.\|\boldsymbol{MN}\|^2 + \|\boldsymbol{n}_M - \boldsymbol{n}_N\|^2$$

where α is a weighting coefficient for normalisation.

This double definition of a point (location + direction) refines the matching criterion and makes it more robust and precise. However, such features must be used with caution, especially when trying to define a distance between two features. [20] will be the basis for a further investigation.

2.4 Computing an optimal 3D-planispheric coordinate system

A keypoint in the estimation of the 4D transformation is the definition of a 3D-planispheric coordinate system (a center, a base, an apico-basal vector, a septo-lateral vector and a normalisation factor σ_r).

2.4.1 The coordinate system

In [8], we define a method to align a SPECT heart image with a template using a non-rigid transformation. This method gives a transformation from the normalized coordinates of the template to the patient's case.

As soon as the transformation that deforms the template is sufficiently free (B-spline tensor product), the template can be chosen as a rough approximation of a LV. Here, we chose two truncated ellipsoids (one for the endocardium and one for the epicardium). The parameters have been set manually not to design a precise shape: the idea is just to have a "good-looking" one. We define for this template a center, a basis point and a point in the lateral wall so that all three define a reference system $[C, \boldsymbol{u}, \boldsymbol{v}]$.

The template is matched with the edges of the image of the heart at end diastole (largest volume). With this transformation, we deform the reference system of the template to the patient case.

Calling S (for "shape") the spline transformation deforming the template to the patient's case, the reference system is defined as follows:

- For the template
  - center: C_T
  - base: B_T
  - lateral point : L_T
  - apicobasal vector : $\boldsymbol{u}_T = \frac{\boldsymbol{C_T B_T}}{\|\boldsymbol{C_T B_T}\|}$
  - septo-lateral vector : $\boldsymbol{v}_T = \frac{\boldsymbol{C_T L_T}}{\|\boldsymbol{C_T L_T}\|}$ (L_T is such that $\boldsymbol{u}_T.\boldsymbol{v}_T = 0$)
  - infero-anterior vector : $\boldsymbol{w}_T = \boldsymbol{u}_T \times \boldsymbol{v}_T$
- For the patient's case
  - center : $C_P = S(C_T)$
  - base : $B_P = S(B_T)$
  - lateral point : $L_P = S(L_T)$
  - apicobasal vector : $\boldsymbol{u}_P = \frac{\boldsymbol{C_P B_P}}{\|\boldsymbol{C_P B_P}\|}$

– septo-lateral vector : $\boldsymbol{v}_P = \frac{\boldsymbol{C_P B_P} - <\boldsymbol{u}_P | \boldsymbol{C_P B_P}> . \boldsymbol{u}_P}{\| \dots \|}$ (so that $\boldsymbol{u}_P . \boldsymbol{v}_P = 0$)

– infero-anterior vector : $\boldsymbol{w}_P = \boldsymbol{u}_P \times \boldsymbol{v}_P$

2.4.2 Choosing σ_r

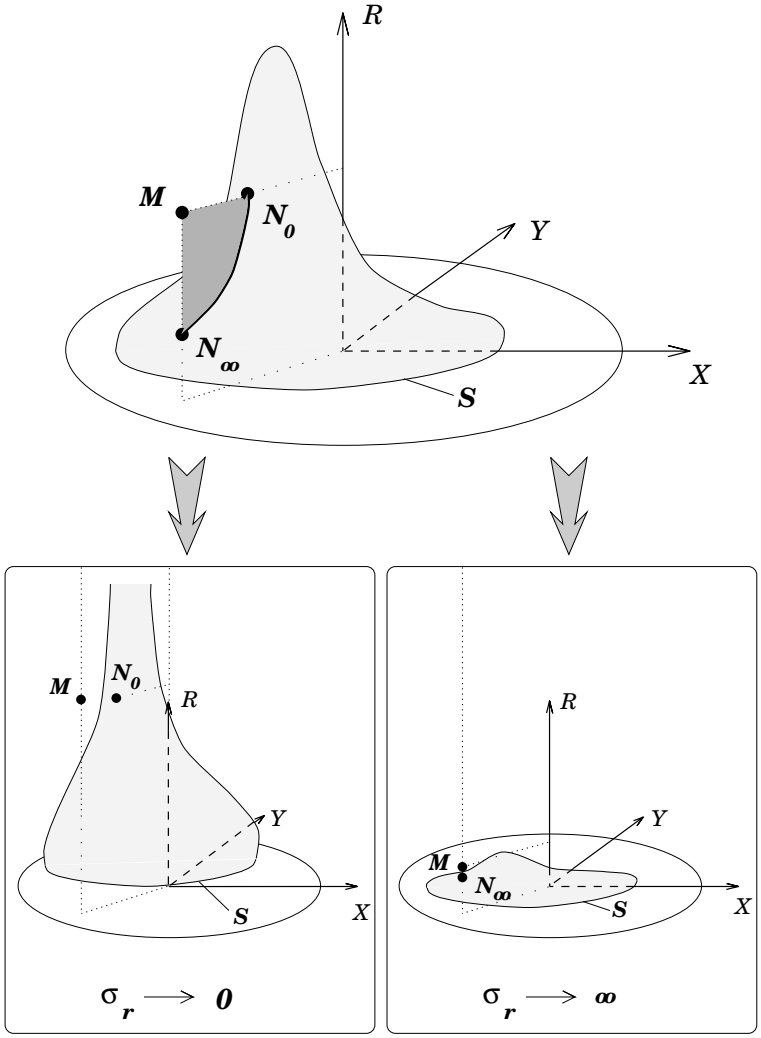

Figure 7: The surface S is represented in planispheric coordinates. In this geometry, the location of the closest point N to M of surface S depends on σ_r. N belongs to the curved segment $[N_0 N_\infty]$, where N_0 and N_∞ are the closest point to M for $\sigma_r = 0$ and ∞ respectively.

The normalisation factor σ_r is used to make the R coordinate dimensionless, as are the other coordinates X and Y. Changing σ_r changes the shape of a surface in the planispheric

geometry by a scaling in the R direction (the lower σ_r, the "higher" the surface). The closest point in this surface to a given point M varies with σ_r (Fig. 7):

- When σ_r approaches 0, the R value becomes very large compared to X and Y, the closest point to M N_0 tends to a point with the same R (Fig. 7, right). This implies that if we use those matches for the least square criterion on distances, the tangential motions (those which change only X and Y) are privileged and the centripetal motion (those which change only R) becomes negligible.
- When σ_r tends to infinity, the R value becomes very small compared to X and Y. The closest point to M N_∞ is a point with same X and Y. This implies that if we use those matches for the least square criterion on distances, the centripetal motion is privileged and the tangential motions are negligible.

Giving a value to this factor therefore amounts to choosing a weighting between purely tangential and purely centripetal motions.

As soon as the latitude of the basal points approaches $\pi/2$, the absolute values of X and Y do not exceed 0.5. For an average heart, it appears that the maximum distance (meaning the r value) of a point of the myocardium to the axis does not exceed CB. We thus choose $\sigma_r = 2.CB$, so that R does not exceed 0.5 as for X and Y. This is an empirical choice which requires a further investigation.

3 Experiments

3.1 Synthetic example

We build here a realistic synthetic example in order to show how an average cardiac motion can be retrieved with the 4D polar transformation.

3.1.1 The synthetic heart

We define two truncated ellipsoids featuring the boundaries of the LV wall. The motion is created by animating the ellipsoids with the motion parameters given in [18]. In this paper, motion parameters (contractions in septo-lateral, antero-inferior and long axis directions, long-axis rotation) are computed from tagged MRI-SPAMM data and displayed for different altitudes on the long axis, one set of curves for each sampled time and for each boundary. These parameters animate a more sophisticated superquadric-based volumetric model of the LV, but our purpose was only to define a simple synthetic model for our experiments, more based on real motion than on a realistic shape.

The center of the synthetic LV is located at [32, 32, 32] (arbitrary units), the semi-axes of the ellipsoids are (8, 4, 4) for the inner boundary and (11, 8, 8) for the outer. The ellipsoids

are truncated at 120 degrees around the base. Those values were chosen arbitrarily, in order to have a "visually reasonable" shape. The parameters of the motion are provided just for the contraction.

3.1.2 Retrieval of trajectories

For the transformation, we set $\boldsymbol{CB} = 6\boldsymbol{y}$. In Fig. 9, $C = [32, 30, 32]$ and the axes of the transformation match the axes of the ellipsoids ($\boldsymbol{u} = [0, 1, 0]$, $\boldsymbol{v} = [0, 0, 1]$). It is non-periodic, the weighting coefficients $\alpha_{n,l}$ are chosen to 1.

The estimated transformation is correct (mean error of 0.052, standard deviation of 0.036, maximum error of 0.19 for an approximate displacement of around 3 units for this particular point[3], with $n_r = 2$, $n_\theta = 3$, $n_\phi = 6$, $n_t = 3$ (which gives 429 control points).

3.1.3 Analysis of the motion

We illustrate in Fig. 10 our decomposition of the displacement in 3 canonical motions characterised by the centripetal contraction, the twist and the elevation, the parameters are drawn at end-systole. The values of the parameters are normalized (between the extremal values: 0 and 0.35 for the contraction, -11 and 4 degrees for the twist and -0.45 and -0.08 for the elevation).

We can see in this figure that the canonical parameters evolve smoothly on the surfaces with respect to θ and ϕ.

- The contraction is more important on the epicardium and maximal around the septum and the lateral wall.
- The twist is roughly uniform around the apico-basal axis and its value increases from -11 degrees at the apex to around 4 degrees at the base. The twist is more important on the endocardium.
- The elevation ratio is roughly constant on the epicardium and is at its minimum around the apex.

Those estimations match the values of the synthetic example.

3.2 Gated SPECT example

We present here experiments conducted on a healthy heart with a gated SPECT images sequence 64x64x64x8 (with Tc 99m radioactive label). This image was provided by Pr. M.L. Goris, Stanford University Hospital (California, USA).

[3]This distance actually corresponds to the maximum displacement of a point from end-diastole to end-systole.

3.2.1 Extraction of feature points

Each image of the sequence is resampled in the polar geometry defined in [8]. In this geometry, the heart looks like a thick plate (Fig. 4). We detect edges in this image with a Canny-Deriche recursive filter [16]. The reason for using such a geometry to find the edges is that cardiac boundary points are easily detected. In an ideal situation, where the heart is a volume of pixels with high intensity values in an image with a high signal-to-noise ratio, starting from the center of the cavity along a radius, the first edge is assumed to belong to the endocardium, the following edge is assumed to belong to the epicardium (Fig. 8).

This heuristic constraint is used to filter out the non-cardiac edges (in SPECT images, there may be some parts of the liver, or artificial edges generated by binary masks). Figure 11 shows the result of the extraction of feature points on four different times of a gated SPECT sequence.

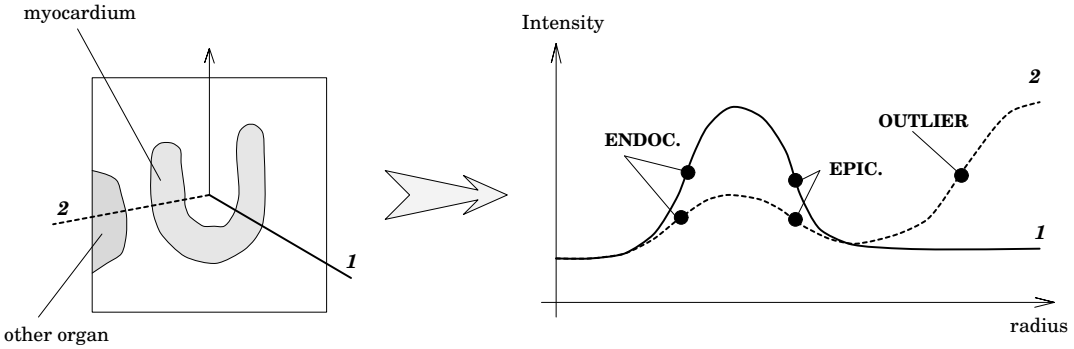

Figure 8: Intensity profiles along 2 different radii starting from the center of the image. The black dots show on both curves the edges detected with the Canny-Deriche filter. On curve 2, the non-cardiac edge is rejected.

3.2.2 Retrieval of trajectories

From these data points, we look for a periodic 4D polar transformation with $n_r = 2$, $n_\theta = 3$, $n_\phi = 6$, $n_t = 5$ (which gives 715 control points, for roughly 50000 data points). Fig. 12 shows the surface of the LV deformed by the 4D polar transformation. This is the surface of a template matched with the method defined in [8]. Because the feature points we extract from the images are not structures, it is difficult to visualise them efficiently. The trajectories of the points are smooth and periodic, as illustrated by Fig. 13.

3.2.3 Analysis of the motion

We show in Fig. 14 a display of the physical parameters values on the surfaces of the heart. For the centripetal contraction, the values vary between 0 and 40 %, for the elevation, between -5 % and 5 % and for the apico-basal rotation, from -10 to 10 degrees.

In Fig. 15, we show a display of the amplitude and the phase of the first harmonic of the centripetal contraction. This crude Fourier analysis shows how the parameter varies over the whole sequence:

- the amplitude shows how wide is this motion, revealing that the inner boundary contracts more than the outer boundary,
- the phase shows the synchronisation of the contraction. On this example (Fig. 15), the phase is higher in the septum (around 20 degrees) than in the other walls. This slight shift of phase confirms the visual impression while observing the sequence.

Those values must be interpreted with caution. As soon as the matching procedure works with a closest point method, the tangential motions which are retrieved are not reliable (elevation and apico-basal rotation). As a matter of fact, only the centripetal contraction (an "orthogonal" motion) matches what can be expected from a healthy heart [18, 28].

3.3 Perspectives for the validation

The motion we are able to retrieve and analyse using gated-SPECT images sequences must be interpreted with caution. Due to the low resolution of the images, it is difficult to get a precise information. Second, any tangential motion cannnot be safely retrieved using only feature-based techniques without markers. The parameters we are able to compute may be useful if there is a possibility to demonstrate that they can be used for a detection of a pathology, by separating normal and abnormal hearts into two statistically different classes. This validation should be processed on a dataset of heart images of which the pathology or healthy state is known. For a given database, the sensitivity and the specificity can be calculated and can show the usefulness of our approach on a quantitative basis.

Another way to validate our decomposition of the motion is to check that it corresponds to a real motion. Tagged MRI yields images in which the motion of soft tissues at a number of discrete points is easily detectable, can be measured [9, 13, 28, 27] and then compared to our computed motion.

These two validation processes are currently under study and will be the subject of a forthcoming article.

4 Conclusion

In this work, the mathematical framework for a new class of transformation is defined: a 4D planispheric transformation is a differentiable function in space and time coordinates and potentially periodic in time. A small number of parameters constrain the definition of the function and there is a simple relationship between the estimated parameters a_p and the "canonical" motions defined for a moving LV (centripetal contraction, rotation, elevation). We demonstrated the feasability of the method on a synthetic example and experimented it on a gated SPECT sequence.

This will be the basis for a number of experimental studies both on nuclear medicine and tagged MR data in collaboration with Pr. Michael Goris (Stanford University Hospital) and Dr. Elliot McVeigh (Johns Hopkins University).

In order to refine the tracking procedure, we are also working on defining feature points **inside** the myocardium. Those points added to the edges we have already defined will give landmarks in the entire myocardial volume and not only on its boundary.

5 Acknowledgements

We want to thank Pr. Michael L. Goris for his precious advices we had and the team of the Stanford University Hospital (California, USA) for providing us with the images.

We give also special thanks to Dr. Eric Bardinet and Pr. Mike Brady for the constructive discussions and comments about the project.

This work was partially supported by regional grant of the Région Provence Alpes Côte d'Azur (doctoral research contract).

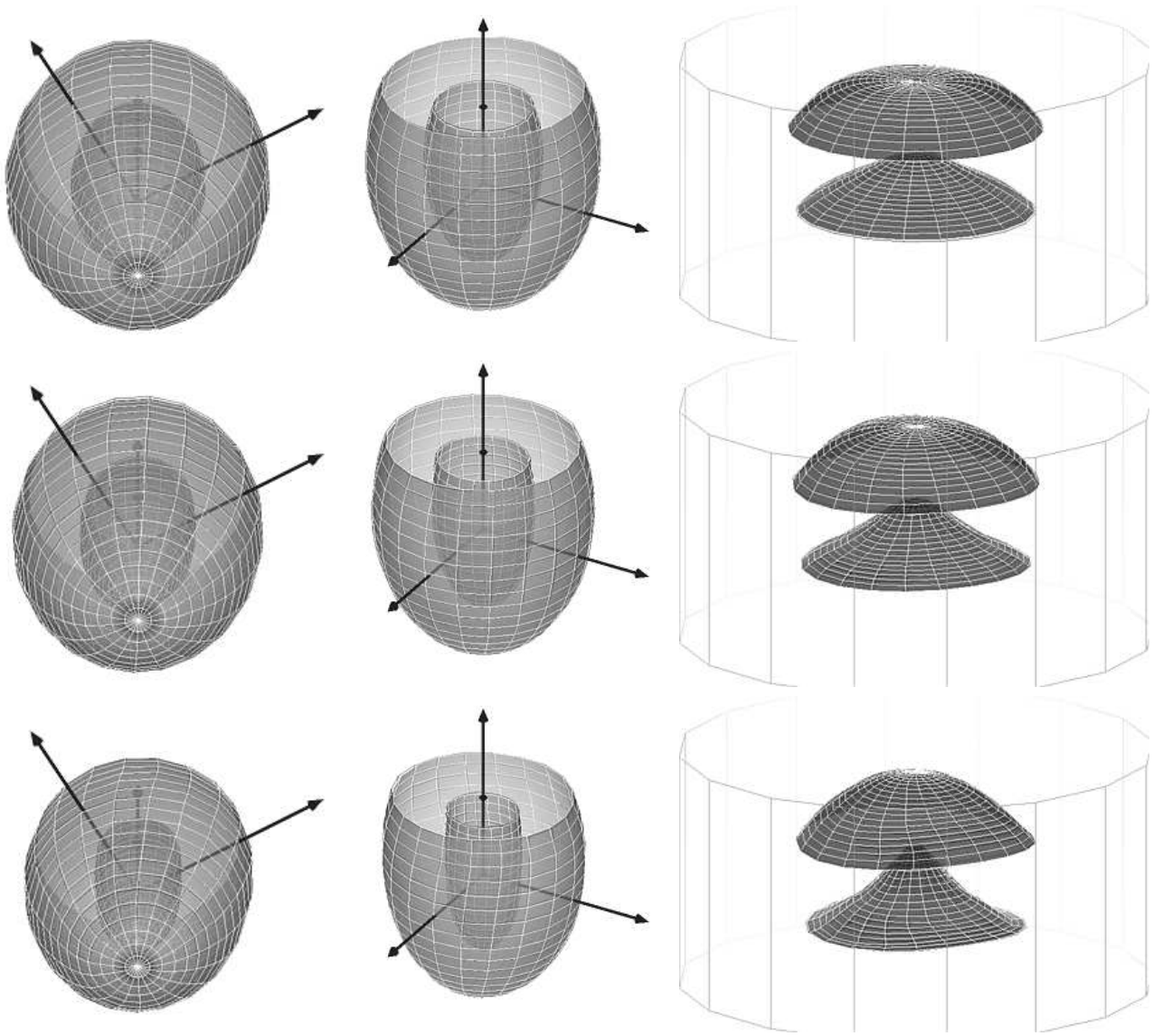

Figure 9: From **top** to **bottom**, different views of the synthetic heart during the contraction. **Left**, from the base, **middle**, from the apex. **Right**, the model in the planispheric coordinate. The mesh representing the original data is outlined in white. The estimated deformed model is represented in dark gray (it is hardly visible under the white mesh).

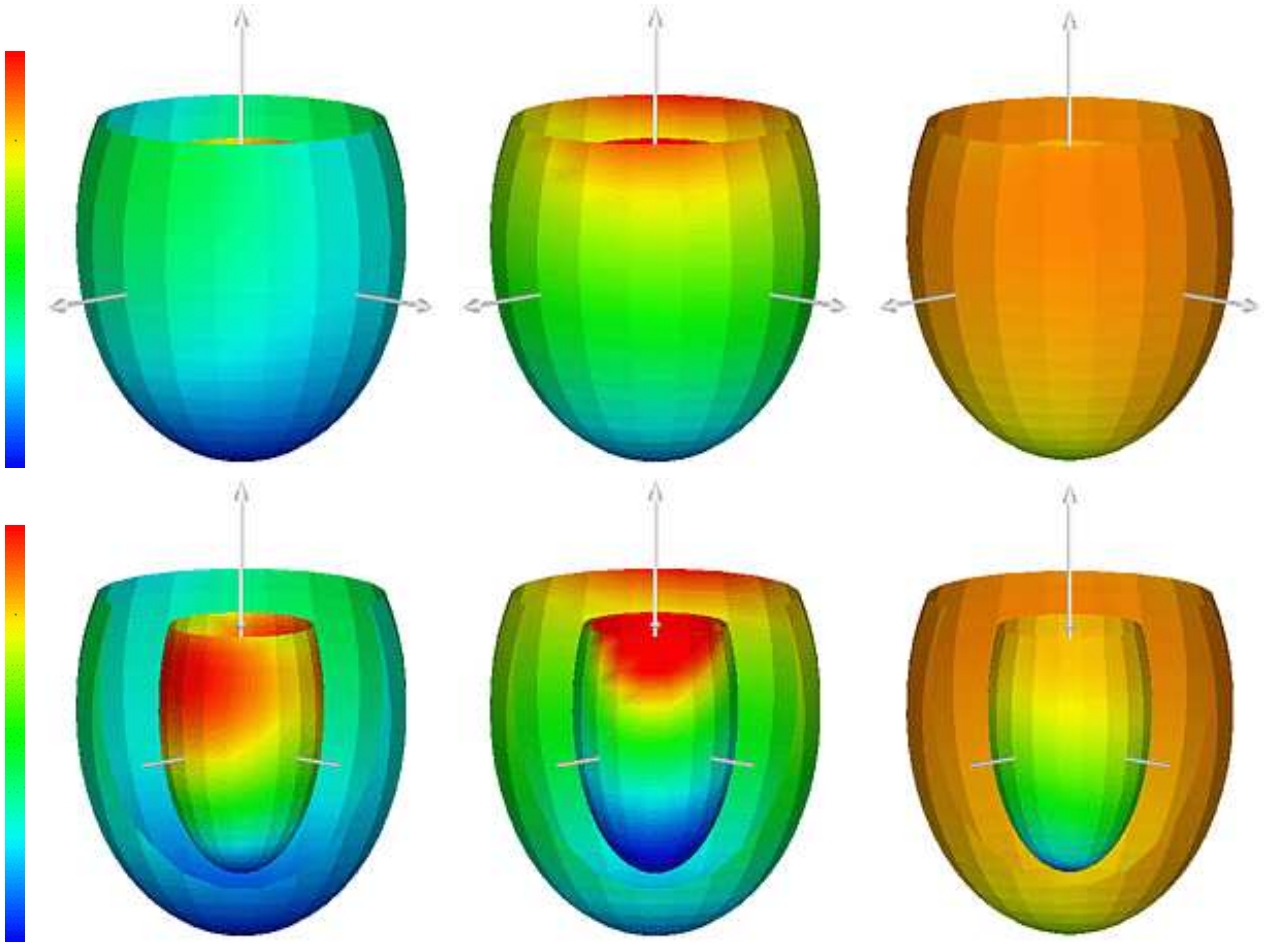

Figure 10: Different views of the synthetic heart at end-diastole colorised with the parameters value. **Left**, centripetal contraction, **middle**, twist, **right**, elevation. The color scale starts from cold colors (blue, green) to hot colors (yellow, red).

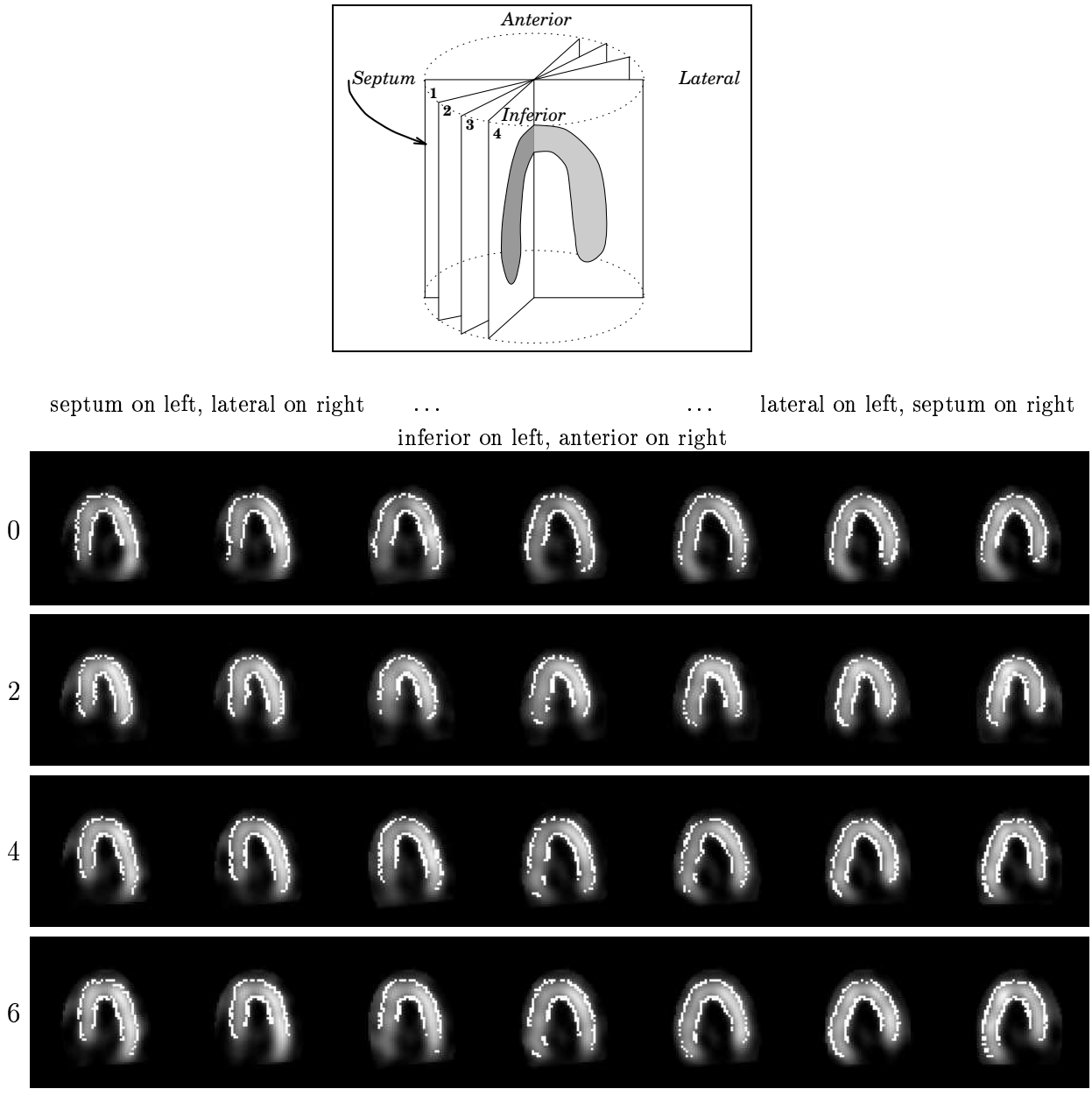

Figure 11: Edges (in white) automatically extracted and filtered from images at four different times (one patient per row, times 0, 2, 4, 6). On each row, we see central slices resampled from the 3D image by rotation around the apex-base axis, as shown on **top** drawing. This makes easier the display of the myocardial structure.

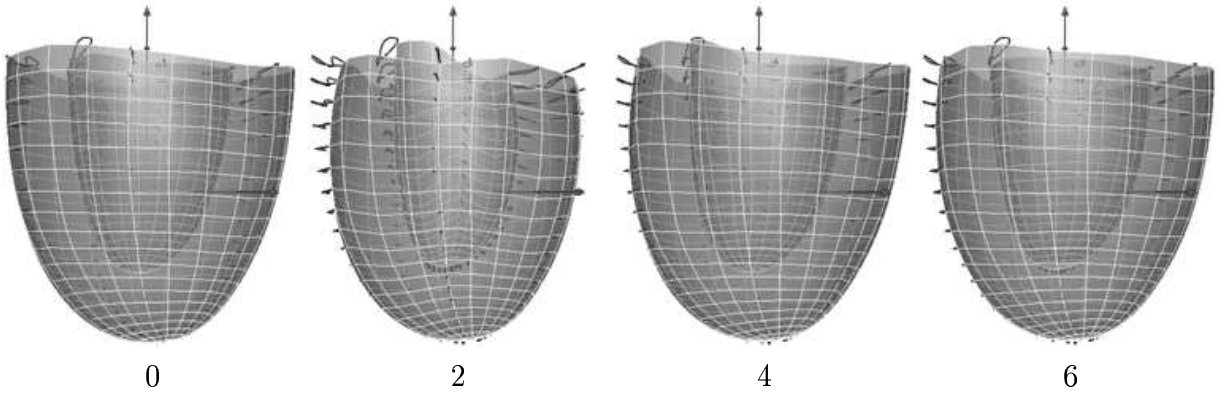

Figure 12: The gated SPECT sequence: from **left** to **right**, times 0, 2, 4, 6. The surface of the LV is outlined in white. Trajectories are represented for some points. In dark gray, the axes of the planispheric coordinate system.

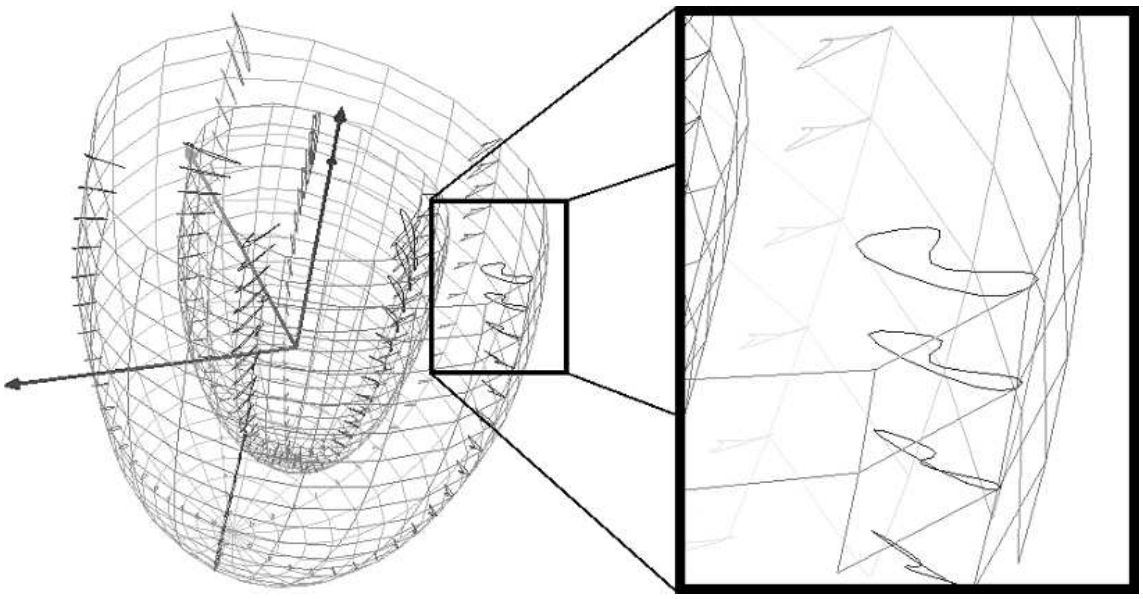

Figure 13: View of the LV from the apex. In dark green, trajectories of some points during the sequence: they are smooth and periodic (see the zoomed area on the right).

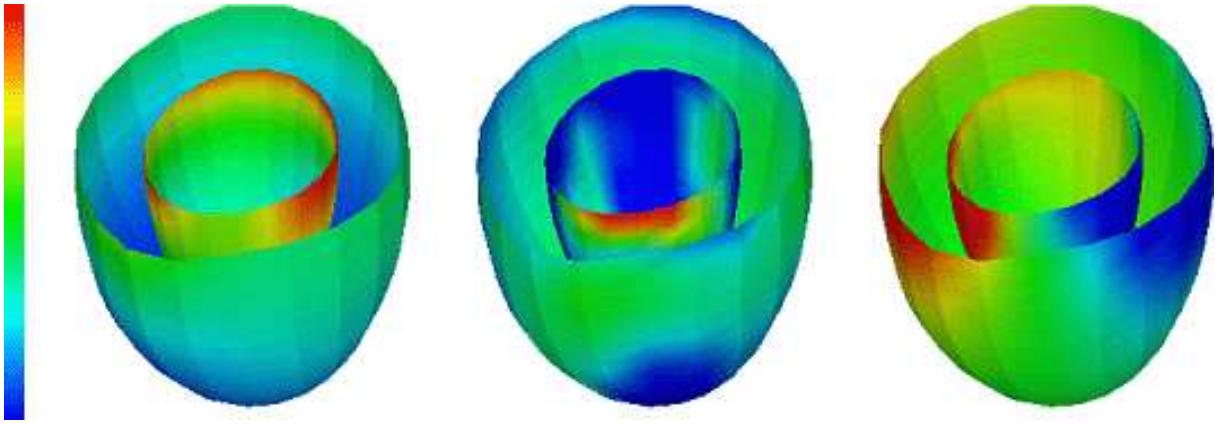

Figure 14: The surface of the heart (septum on the left) colorised with the parameters values at end systole: **left**, the centripetal contraction, **middle**, the elevation and **right**, the apico-basal rotation. **Top right**, the colorscale indicates decreasing values from top to bottom.

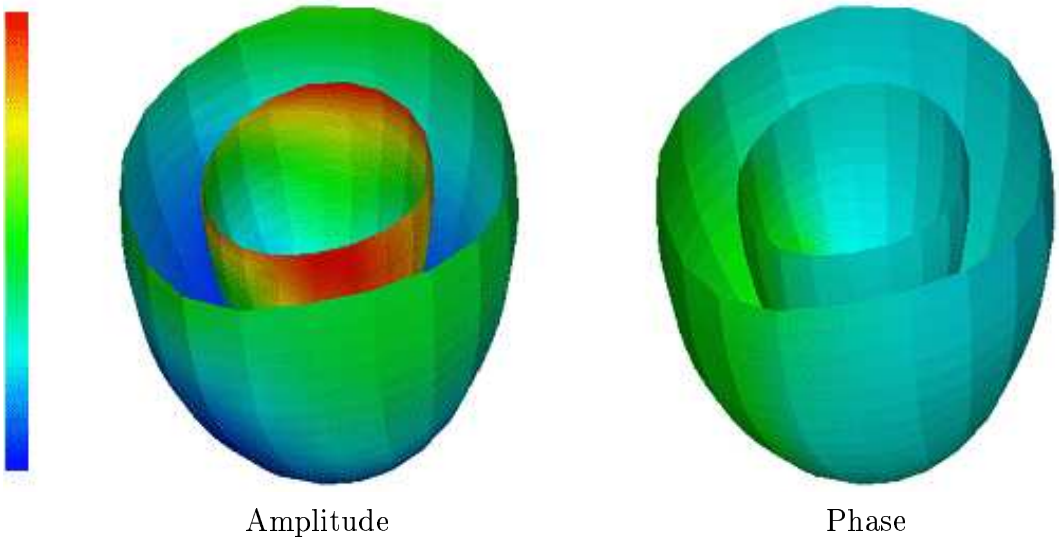

Figure 15: The surface of the heart (septum on the left) colorised with the amplitude (**left**) and phase (**right**) of the first harmonic of the centripetal contraction. **Top right**, the colorscale indicates decreasing values from top to bottom. The amplitude shows how wide the motion is, the phase shows the synchronisation of the contraction: here, the septum starts contracting later than the other walls.

A 3D planispheric coordinate

This section is dedicated to the problem of finding H_M given a point M in space. In order to avoid cumbersome notation, we rename H_M as H. The problem is, given two points C and B and a point M, to find a point H on the line CB so that:

$$\begin{aligned}(\boldsymbol{BC}, \boldsymbol{HM}) &= \theta \\ \boldsymbol{CH} &= (1 - cos\theta).\boldsymbol{CB}\end{aligned}$$

Let us define λ as follows:

$$\overline{CH} = \lambda.\overline{CB} = \lambda.l$$

Because λ is supposed to be equal to $1 - cos(\theta)$, $\lambda \in [0, 2]$.

If we write

$$\boldsymbol{CM} = \begin{pmatrix} x.l \\ y.l \\ z.l \end{pmatrix} \qquad \text{and} \qquad \boldsymbol{u} = \begin{pmatrix} u_x \\ u_y \\ u_z \end{pmatrix}$$

we have

$$\boldsymbol{HM} = l.\begin{pmatrix} x - \lambda.u_x \\ y - \lambda.u_y \\ z - \lambda.u_z \end{pmatrix}$$

so

$$\begin{aligned}\boldsymbol{u}.\boldsymbol{HM} &= \boldsymbol{u}.\boldsymbol{HC} + \boldsymbol{u}.\boldsymbol{CM} \\ &= l.[-\lambda + (x.u_x + y.u_y + z.u_z)]\end{aligned}$$

On the other hand,

$$cos(\theta) = \frac{\boldsymbol{BC}.\boldsymbol{HM}}{\|\boldsymbol{BC}\|.\|\boldsymbol{HM}\|}$$

If we call

$$\begin{aligned}r &= \|\boldsymbol{HM}\| \\ &= l.\sqrt{(x - \lambda.u_x)^2 + (y - \lambda.u_y)^2 + (z - \lambda.u_z)^2}\end{aligned}$$

and

$$p = \boldsymbol{u}.\boldsymbol{CM}$$

we thus have

$$cos(\theta) = -\frac{\boldsymbol{u}.\boldsymbol{HM}}{r}$$

and the constraint (1) can be rewritten, after some calculation,

$$\lambda = \frac{r+p}{r+1} \tag{12}$$

Let us call f a function of λ

$$f(\lambda) = \frac{r(\lambda)+p}{r(\lambda)+1} - \lambda \tag{13}$$

We look for λ_0 so that

$$f(\lambda_0) = 0 \tag{14}$$

To solve this equation, we use a Newton method. In the following lines, we demonstrate that the derivative f' is of a constant sign, which implies a unique solution for (14), if it exists.

The derivative of the function f with respect to λ is as follows

$$f'(\lambda) = \frac{r'(\lambda)(1-p)}{(r(\lambda)+1)^2} - 1$$

It is straightforward to prove that

$$r'(\lambda) = \frac{\lambda - p}{r(\lambda)}$$

so we have

$$f'(\lambda) = \frac{(\lambda-p)(1-p)}{r(\lambda)(r(\lambda)+1)^2} - 1 \tag{15}$$

Let us call M' is the projection of M on (CB). We have then

$$\lambda - p = -\frac{\overline{HM'}}{l}$$
$$1 - p = -\frac{\overline{BM'}}{l}$$

To prove the constant sign of f', we just have to compare the two distance products $CB.\overline{HM'}.\overline{BM'}$ (the numerator of the fraction) and $HM.(HM+CB)^2$ (the denominator of the fraction). If we can prove that $CB.\overline{HM'}.\overline{BM'} < HM.(HM+CB)^2$, the fraction is lower than 1 and f' is negative.

Due to the symmetry of the problem, we can suppose without any loss of generality that M' is on the semi-line $[BC)$. The demonstration of the inequality splits in two parts:

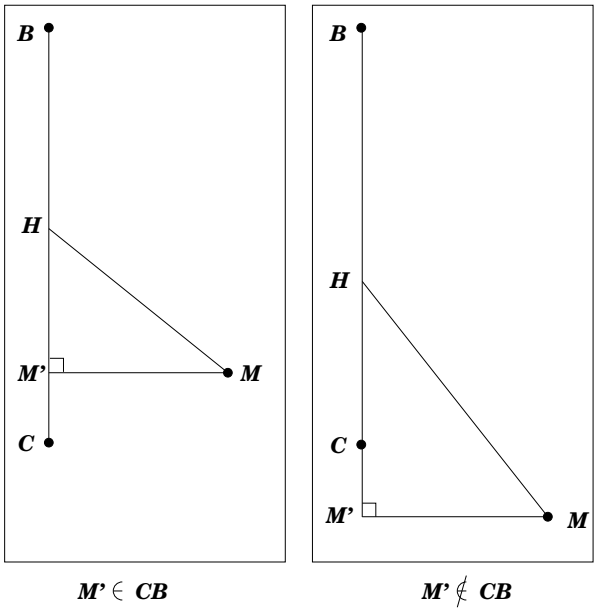

Figure 16: Two possible configurations for M'.

- $M' \in [CB]$ (Fig. 16, left). We obviously have

$$\begin{array}{rcccl} M'B & < & CB & < & HM + CB \\ CB.M'B & < & CB^2 & < & (HM + CB)^2 \end{array}$$

as $HM' < HM$,

$$CB.HM'.M'B < HM.(HM + CB)^2$$
$$CB.\overline{HM'}.\overline{BM'} < HM.(HM + CB)^2$$

this what we want.

- $M' \notin [CB]$ (Fig. 16, right). We have

$$\begin{array}{rcl} (HM + CB)^2 & > & (HM' + CB)^2 \\ & > & (CM' + CB)^2 = M'B^2 \\ & > & M'B.CB \end{array}$$

as $HM' < HM$,

$$CB.HM'.M'B < HM.(HM + CB)^2$$
$$CB.\overline{HM'}.\overline{BM'} < HM.(HM + CB)^2$$

this what we want.

So, in any configuration of M, for any λ, $f'(\lambda) < 0$. f is then a decreasing function. Obviously,

$$f(0) = \frac{CM + \boldsymbol{u}.\boldsymbol{CM}}{CM + CB} > 0$$

and, if M' is on the semi-line $[BC)$,

$$\begin{aligned} f(1) &= \frac{BM + \boldsymbol{u}.\boldsymbol{CM}}{BM + CB} - 1 \\ &= \frac{\boldsymbol{u}.\boldsymbol{CM} - CB}{BM + CB} \\ &= \frac{\boldsymbol{u}.\boldsymbol{BM}}{BM + CB} < 0 \end{aligned}$$

$f(0)$ and $f(1)$ are of opposite signs, the sign f' is constant, there is then a unique solution for (14).

In our implementation, we use a Newton method to find λ_0 solution of (14). Starting from a central position ($\lambda = 1$), after 3 or 4 iterations, the difference between two successive estimations of λ do not exceed 10^{-6}. The convergence is extremely fast.

References

[1] A. Amini and J. Duncan. Bending and Stretching Models for LV wall Motion Analysis from Curves and Surfaces. In *Image and Vision Computing*, volume 10, pages 418–430, August 1992.

[2] T. Arts, W.C. Hunter, A. Douglas, A.M. Muijtjens, and R.S. Reneman. Description of the deformation of the left ventricle by a kinematic model. *Journal of Biomechanics*, 25(10):1119–1127, 1992.

[3] E. Bardinet, L.D. Cohen, and N. Ayache. Tracking medical 3D data with a parametric deformable model. In *IEEE Computer Vision Symposium*, November 1995.

[4] E. Bardinet, L.D. Cohen, and N. Ayache. Tracking and motion analysis of the left ventricle with deformable superquadrics. *Medical Image Analysis*, 1(2), 1996. (also INRIA research report #2797).

[5] S. Benayoun, C. Nastar, and N. Ayache. Dense Non-rigid Motion Estimation in Sequences of 3D Images Using Differential Constraints. In *Computer Vision, Virtual Reality and Robotics in Medicine*, volume 905 of *Lecture Notes in Computer Science*, pages 309–318. Springer-Verlag, April 1995.

[6] P. Besl and N. McKay. A Method for Registration of 3D Shapes. *IEEE Transactions on Pattern Analysis and Machine Intelligence*, 14:239–256, February 1992.

[7] P. Clarysse, O. Jaouen, I. Magnin, and J.M. Morvan. 3D Boundary Extraction of the Left Ventricle by a Deformable Model with a priori Information. In *IEEE International Conference on Image Processing*, October 1995.

[8] J. Declerck, J. Feldmar, M.L. Goris, and F. Betting. Automatic Registration and Alignment on a Template of Cardiac Stress & Rest SPECT Images. In *Mathematical Methods in Biomedical Image Analysis*, June 1996. (Also INRIA Research Report # 2770).

[9] T.S. Denney Jr and J.L. Prince. 3D Displacement Field Reconstruction from Planar Tagged Cardiac MR Images. In *IEEE Workshop on Biomedical Image Analysis*, pages 51–60, June 1994.

[10] J. Feldmar and N. Ayache. Rigid, Affine and Locally Affine Registration of Free-Form Surfaces. *International Journal of Computer Vision*, In press. (Also INRIA Research Report # 2220).

[11] D. Goldgof, H. Lee, and T. Huang. Motion Analysis of Non-rigid Surfaces. In *IEEE Computer Vision and Pattern Recognition*, pages 375–380, 1988.

[12] P.J. Hunter and B.H. Smaill. The Analysis of Cardiac Function: a Continuum Approach. *Programming in Biophysics and Molecular Biology*, 52:101–164, 1988.

[13] D. Kraitchman, A. Young, C.N. Chang, and L. Axel. Semi-Automatic Tracking of Myocardial Motion in MR Tagged Images. *IEEE Transactions on Medical Imaging*, 14(3):422–433, September 1995.

[14] J.C. McEachen, A. Nehorai, and J.S. Duncan. A Recursive Filter for Temporal Analysis of Cardiac Motion. In *IEEE Workshop on Biomedical Image Analysis*, pages 124–133, June 1994.

[15] F.G. Meyer, R. Todd Constable, A. Sinusas, and J. Duncan. Tracking Myocardial Deformation Using Spatially-Constrained Velocities. In Y. Bizais et al., editor, *Information Processing in Medical Imaging*, pages 177–188, 1995.

[16] O. Monga, R. Deriche, and J.M. Rocchisani. 3D edge detection using recursive filtering: application to scanner images. *Computer Vision Graphics and Image Processing*, January 1991.

[17] C. Nastar. Vibration Modes for Non-Rigid Motion Analysis in 3D Images. In *European Conference in Computer Vision*, May 1994.

[18] J. Park, D. Metaxas, and L. Axel. Analysis of left ventricular motion based on volumetric deformable models and MRI-SPAMM. *Medical Image Analysis*, 1(1):53–71, March 1996.

[19] J. Park, D. Metaxas, and A. Young. Deformable Models with Parameter Functions : Application to Heart-Wall Modeling. In *IEEE Computer Vision and Pattern Recognition*, pages 437–442, June 1994.

[20] X. Pennec and N. Ayache. Randomness and Geometric Features in Computer Vision. In *IEEE Conf. on Computer Vision and Pattern Recognition (CVPR'96)*, San Francisco, Cal, June 1996.

[21] P. Radeva, A. Amini, J. Huang, and E. Marti. Deformable B-Solids and Implicit Snakes for Localization and Tracking of MRI-SPAMM Data. In *Mathematical Methods in Biomedical Image Analysis*, June 1996.

[22] J.-J. Risler. *Méthodes Mathématiques pour la CAO*. Masson, 1991.

[23] P. Shi, A. Amini, G. Robinson, A. Sinusas, C.T. Constable, and J. Duncan. Shape-Based 4D Left Ventricular Myocardial Function Analysis. In *IEEE Workshop on Biomedical Image Analysis*, pages 88–97, June 1994.

[24] P. Shi, G. Robinson, A. Chakraborty, L. Staib, R. Constable, A. Sinusas, and J. Duncan. A Unified Framework to Assess Myocardial Function from 4D Images. In *Computer Vision, Virtual Reality and Robotics in Medicine*, volume 905 of *Lecture Notes in Computer Science*, pages 327–337. Springer-Verlag, April 1995.

[25] J.-P. Thirion. Fast Non-rigid Matching of 3D Medical Images. In *Medical Robotics and Computer Aided Surgery*, pages 47–54, November 1995.

[26] R.T. Todd Constable, K.M. Rath, A.J. Sinusas, and J.C. Gore. Development and Evaluation of Tracking Algorithms for Cardiac Wall Motion Analysis Using Phase Velocity MR Imaging. In *Magnetic Resonance Medicine*, volume 32, pages 33–42, 1994.

[27] A. Young, D. Kraitchman, L. Dougherty, and L. Axel. Tracking and Finite Element Analysis of Stripe Deformation in Magnetic Resonance Tagging. *IEEE Transactions on Medical Imaging*, 14(3):413–421, September 1995.

[28] A.A. Young, C.K. Kramer, V.A. Ferrari, L. Axel, and N. Reichek. Three-Dimensional Left Ventricular Deformation in Hypertrophic Cardiomyopathy. *Circulation*, 90:854–867, August 1994.

[29] Z. Zhang. Iterative point matching for registration of free-form curves and surfaces. *International Journal of Computer Vision*, 13(2):119–152, December 1994. Also INRIA Research Report #1658.

Unité de recherche INRIA Lorraine, Technopôle de Nancy-Brabois, Campus scientifique,
615 rue du Jardin Botanique, BP 101, 54600 VILLERS LÈS NANCY
Unité de recherche INRIA Rennes, Irisa, Campus universitaire de Beaulieu, 35042 RENNES Cedex
Unité de recherche INRIA Rhône-Alpes, 655, avenue de l'Europe, 38330 MONTBONNOT ST MARTIN
Unité de recherche INRIA Rocquencourt, Domaine de Voluceau, Rocquencourt, BP 105, 78153 LE CHESNAY Cedex
Unité de recherche INRIA Sophia-Antipolis, 2004 route des Lucioles, BP 93, 06902 SOPHIA-ANTIPOLIS Cedex

Éditeur
INRIA, Domaine de Voluceau, Rocquencourt, BP 105, 78153 LE CHESNAY Cedex (France)
ISSN 0249-6399